Sheet-gravel evidence for a late Holocene tsunami run-up on beach dunes, Great Barrier Island, New Zealand

Article *in* Sedimentary Geology · January 2003

DOI: 10.1016/S0037-0738(02)00191-4

CITATIONS
69

READS
110

3 authors, including:

Scott L Nichol
Geoscience Australia
111 PUBLICATIONS **2,373** CITATIONS
SEE PROFILE

Olav B. Lian
University of the Fraser Valley
73 PUBLICATIONS **1,437** CITATIONS
SEE PROFILE

Available online at www.sciencedirect.com
SCIENCE DIRECT®
Sedimentary Geology 155 (2003) 129–145
Sedimentary Geology
www.elsevier.com/locate/sedgeo

Sheet-gravel evidence for a late Holocene tsunami run-up on beach dunes, Great Barrier Island, New Zealand

Scott L. Nichol [a,*], Olav B. Lian [b,1], Charles H. Carter [c]

[a] School of Geography and Environmental Science, University of Auckland, Private Bag 92019, Auckland, New Zealand
[b] School of Earth Sciences, Victoria University of Wellington, P.O. Box 600, Wellington, New Zealand
[c] Department of Geology, University of Akron, Akron, OH, 44325, USA

Received 17 July 2001; accepted 25 March 2002

Abstract

A semi-continuous sheet of granule to cobble-size clasts forms a distinctive deposit on sand dunes located on a coastal barrier in Whangapoua Bay, Great Barrier Island, New Zealand. The gravel sheet extends from the toe of the foredune to 14.3 m above mean sea level and 200 m landward from the beach. Clasts are rounded to sub-rounded and comprise lithologies consistent with local bedrock. Terrestrial sources for the gravel are considered highly unlikely due to the isolation of the dunes from hillslopes and streams. The only source for the clasts is the nearshore to inner shelf of Whangapoua Bay, where gravel sediments have been previously documented. The mechanism for transport of the gravel is unlikely to be storm surge due to the elevation of the deposit; maximum-recorded storm surge on this coast is 0.8 m above mean high water spring tide. Aeolian processes are also discounted due to the size of clasts and the elevation at which they occur. Tsunami is therefore considered the most probable mechanism for gravel transport. Minimum run-up height of the tsunami was 14.3 m, based on maximum elevation of gravel deposits. Optical ages on dune sands beneath and covering the gravel allow age bracketing to 0–4.7 ka. Within this time frame, numerous documented regional seismic and volcanic events could have generated the tsunami, notably submarine volcanism along the southern Kermadec arc to the east-southeast of Great Barrier Island where large magnitude events are documented for the late Holocene. Radiocarbon ages on shell from Maori middens that appear to have been reworked by tsunami run-up constrain the age of this event to post ca. 1400 AD. Regardless of the precise age of this event, the well-preserved nature of the Whangapoua gravel deposit provides for an improved understanding of the high degree of spatial variability in tsunami run-up.

Keywords: Tsunami; Clastic sediments; Gravel deposits; Optical dating; Radiocarbon dating

1. Introduction

Attention to the sedimentary record of prehistoric tsunami in coastal environments has tended to focus on deposits within subaqueous to low-supratidal locations, where preservation potential is high. Compelling evidence from lowland (coastal swamps, freshwater wetlands) to shallow marine (estuaries, lagoons) envi-

* Corresponding author. Fax: +64-9-3737434.
E-mail addresses: s.nichol@auckland.ac.nz (S.L. Nichol), olav.lian@rhul.ac.uk (O.B. Lian), chcarter@uakron.edu (C.H. Carter).
[1] Present address: Centre for Quaternary Research, Department of Geography, Royal Holloway, University of London, Egham, Surrey, TW20 0EX, UK.

0037-0738/02/$ - see front matter © 2002 Elsevier Science B.V. All rights reserved.
PII: S0037-0738(02)00191-4

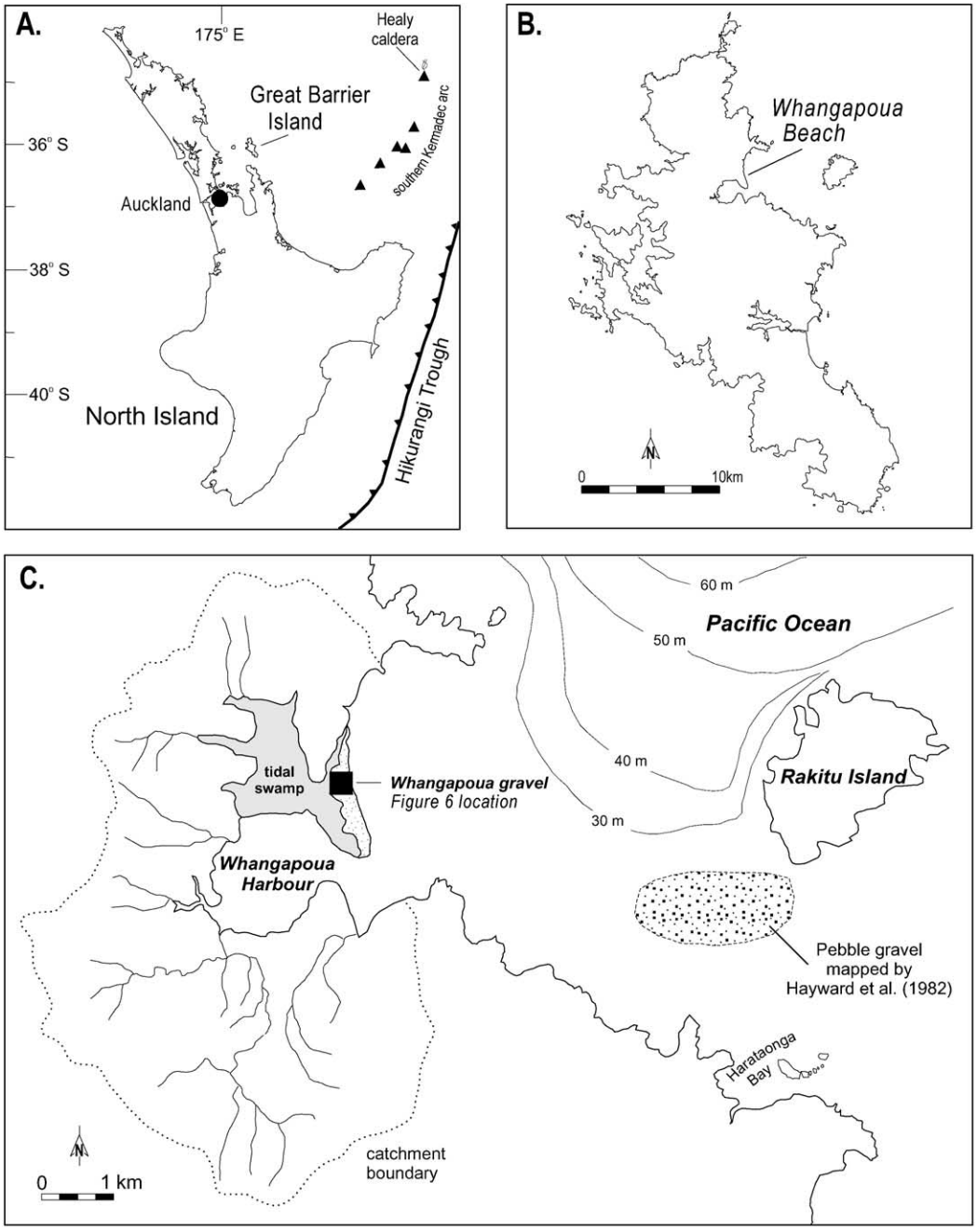

Fig. 1. (A) Location map of Great Barrier Island, northeast New Zealand. Also showing Hikurangi Trough that marks the subduction zone between the Australian and Pacific plates, an area of frequent seismicity in late Holocene time and the position of modern submarine volcanoes along the southern Kermadec arc (after Wright et al., in press). (B) Map of Great Barrier Island showing Whangapoua Harbour. (C) Map of Whangapoua Bay showing offshore bathymetry, study site and the location of submarine gravels, mapped by Hayward et al. (1982, 1986).

ronments has been presented from a variety of locations in regions with a well-documented tsunami record, including: the Pacific southwest of Canada (e.g., Clague, 1997; Clague et al., 2000); the Pacific northwest of the United States (e.g., Atwater, 1987; Atwater et al., 1995); Japan (Minoura and Nakaya, 1991; Minoura et al., 1994; Takashimizu and Masuda, 2000); the Mediterranean (Cita et al., 1984); the eastern Atlantic coast (Dawson et al., 1995); and New Zealand (Goff et al., 2000; Goff and Chagué-Goff, 1999). These records provide good evidence for tsunami propagation and amplification into confined basins or valleys, often with distinctly different sedimentological signatures of tsunami up-rush and backwash but with poor records of run-up height. In contrast, tsunami deposits preserved in subaerial coastal environments such as barriers, dunes and cliff-tops can provide for estimates of (minimum) tsunami run-up elevation (e.g., Bryant et al., 1992, 1996; Young et al., 1996). Observation from recent tsunamis, such as the Flores tsunami of December 1992 (Yeh et al., 1993) and the Papua New Guinea tsunami of July 1998 (McSaveney et al., 2000), demonstrate the high degree of spatial variability in tsunami behaviour on shorelines. In particular, these events produced complex patterns of run-up and backwash that caused localised erosion, semi-continuous re-deposition of sediment and areas of no apparent impact. Numerical models of tsunami run-up have been found to underestimate actual run-up by

Fig. 2. (A) Oblique aerial view of Whangapoua barrier spit. Arrow indicates position of Whangapoua gravel. (B) Foredune behind Whangapoua beach showing the main area of gravel sheet. Dashed line indicates landward and highest limit of Whangapoua gravel. (C) Foredune and gravel sheet viewed from Whangapoua beach. Dashed line indicates maximum limit of storm run-up on dunes. (D) Close view of Whangapoua gravel. Note roundness of larger clasts (spade handle is 0.7 m long).

an order of magnitude (Yeh et al., 1993), which suggests that further collection of empirical data on tsunami run-up remains a priority, particularly via the use of facies analysis as encouraged by Lowe and de Lange (2000).

This paper describes the form and sedimentological character of a coarse-grained clastic tsunami deposit lain down on coastal dunes on Great Barrier Island, New Zealand. Optical ages (optically stimulated luminescence; OSL) from dune sands below and above the gravel are used to constrain the age of deposition, and radiocarbon ages from shells in Maori middens provide a basis for relating the depositional event to a period of early human occupation on this coast. We also discuss the significance of the spatial variability of this particular deposit, in the context of geomorphic controls over patterns in tsunami run-up and consider likely local sources for tsunami generation.

2. Study site

Great Barrier Island is situated in the outer Hauraki Gulf, approximately 100 km to the east of North Island, New Zealand (Fig. 1). The island covers an area of approximately 28,500 ha, with the interior formed in steeply dissected volcanic terrain rising to 620 m above sea level. The basement rocks are predominantly Mesozoic greywackes and shales (Thompson, 1960). The coastline of Great Barrier Island is characterised by numerous embayments and a rocky shoreline, especially on the western coast where bays and inlets have received little sediment. In contrast, a series of lowland freshwater swamps impounded by dunes, and small estuaries occupy part of the eastern coast. The study site for this paper is located on the bay-mouth barrier at the entrance to Whangapoua Harbour, the largest estuary on the eastern coast of Great Barrier Island.

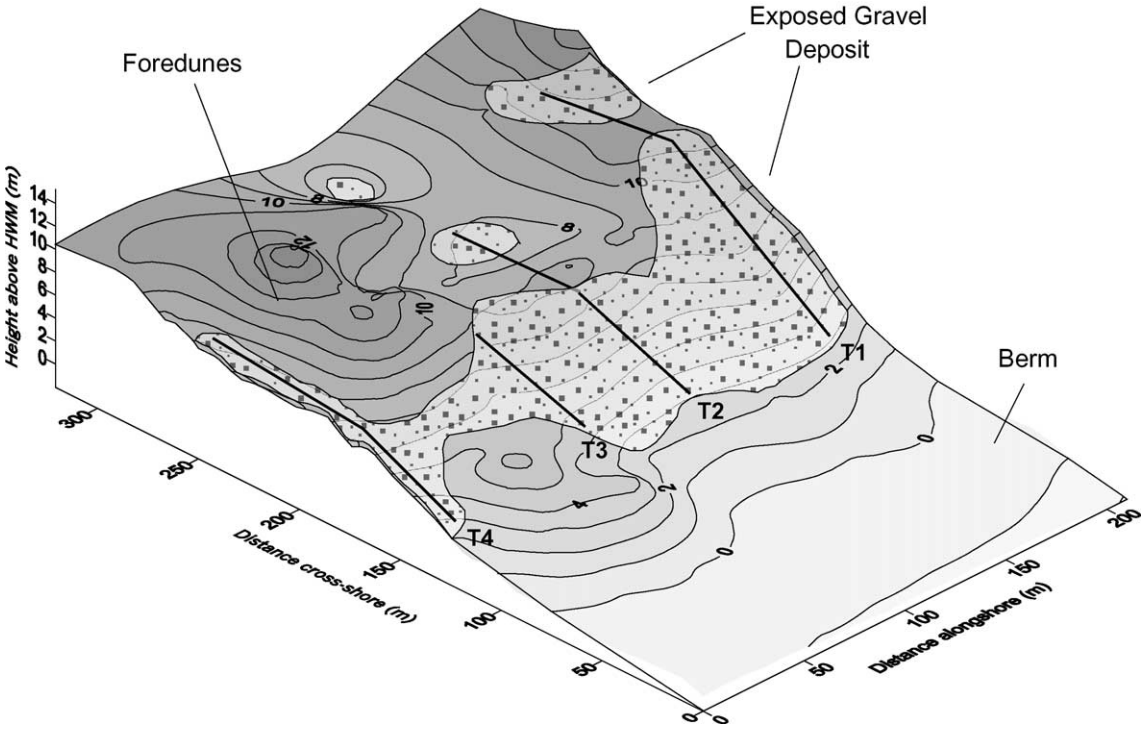

Fig. 3. Three-dimensional plot of the Whangapoua dunes and upper beach, showing the extent of gravel outcrop. Contour interval = 1 m. This area of the dunefield is located mid-way along Whangapoua bay where focusing of tsunami run-up is inferred. T1…T4 denotes cross-shore transects used for gravel size analysis.

Whangapoua Harbour covers an area of 4.5 km^2, with a catchment area of 26.5 km^2 that is drained by a network of 12, mostly ephemeral, streams. Maximum elevation in the catchment is 460 m above sea level. The catchment geology is predominantly weakly stratified andesitic breccias, tuffs and agglomerates, with small areas of rhyolite in the upper catchment, and fractured greywackes plus argillites to the north (Thompson, 1960); these rocks crop out in shore platforms and headlands at both ends of Whangapoua Bay. The present configuration and depositional environments of this coast are presumed to have been established ca. 6.5 ka BP at the termination of post-glacial sea-level rise in New Zealand (Gibb, 1986).

Whangapoua Harbour is partly enclosed on its seaward side by a sandy barrier-spit that is 2 km in length and oriented north to south (Fig. 1). A dune field covers the central section of the barrier, extending a maximum of 300 m landward toward a back-barrier flat of supratidal to intertidal saltmarsh, that in turn grades to mangrove swamp that fringes the harbour. The dune field comprises a primary ridge that is 10–12 m high and characterised by a moderate degree of soil development as indicated by a mid-brown colour. The average seaward slope of the primary dune is 6°. Secondary dunes have developed over the primary ridge, comprising <5 m-high hummocks that are partly vegetated and lack soil development. The primary dune ridge is mantled with a semi-continuous sheet of gravel and pebble- to cobble-sized clasts, herein termed the Whangapoua gravel (Fig. 2). The gravel sheet is one grain thick and extends 200 m landward from the toe of foredunes. In places, secondary transient dunes have formed over the gravel. Maximum elevation of the Whangapoua gravel sheet is 14.3 m above mean sea level and its surface exposure covers an area of approximately 30,000 m^2 (Fig. 3).

Several archaeological sites (shell middens and fire pits) are located within the dune field, and within the area of the Whangapoua gravel sheet. These middens show evidence of reworking, with cultural material (broken shell and hearth stones up to 8 cm long) scattered as discrete sheets up to 10 m landward of primary midden deposits. Also, isolated hearth-stones up to 100 mm in size, are scattered throughout the gravel sheet up to 100 m from existing middens, which due to their angularity and charred appearance are easily distinguished from the Whangapoua gravel (Fig. 4).

The southern half of Whangapoua barrier is characterised by a series of low (<5 m) dunes separated by deflation zones and shallow (<1 m deep) ephemeral (storm) channels. Isolated remnants of older dunes crop out along this southern area, and are distinguished from modern dunes by the degree of soil formation (orange-brown podzolic) and the loosely cemented condition of the sands. In places, these orange-brown dune remnants contain Rotoehu tephra near the surface, which indicates that they formed about 45 ka ago (Lian and Shane, 2000). These Pleistocene remnants rise to 6 m above the surrounding modern dunes and deflation zones, and

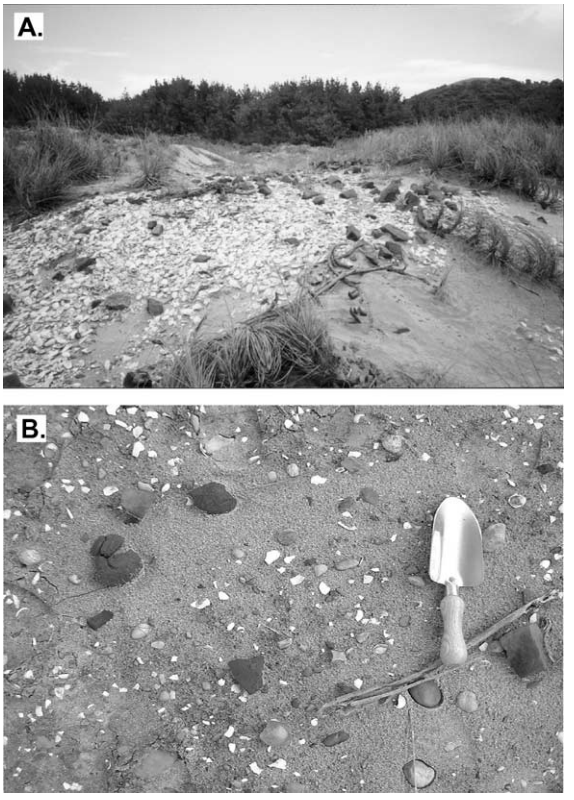

Fig. 4. (A) View of Maori shell midden A at the northern limit of Whangapoua gravel deposits, looking landward. Stones in this photo are hearth stones, which are distinguished from the Whangapoua gravel on the basis of greater angularity and charred surfaces. (B) Angular hearth stones (dark gray) scattered amongst the Whangapoua gravel sheet. This site is approximately 100 m landward of midden A. Trowel is 30 cm long.

are mantled by Whangapoua gravel (Fig. 5). It is important to note that the Pleistocene dunes are clearly not a source for the gravel. We base this on the paucity of gravel, pebble and cobble clasts within the Pleistocene dunes, and the strong contrast in weathering state between the podzolised dune sands and the Whangapoua gravel. The southern tip of the barrier consists of a low berm that grades to tidal flats alongside the inlet to Whangapoua Harbour. This area is regularly inundated during storm surge and floods, but does not feature the gravel deposit.

Offshore from Whangapoua beach, the seabed of the nearshore to inner shelf slopes at 0.8° to 40 m water depth approximately 3 km offshore, where there is an abrupt break in slope to the mid shelf with an average slope of 0.3° (Fig. 1). Rakitu Island is situated 5.8 km offshore, and serves as a point of diffraction and refraction for waves arriving from the north to southeast, and may thus cause focusing of wave energy in the lee of the island, and at Whangapoua beach. A spot survey of the surface sediments from the nearshore (<5 m depth) to the mid shelf (>40 m depth) of northeast Great Barrier Island by Hayward et al. (1982, 1986), documented an extensive cover of well-sorted fine sand but with localised deposits of gravely to pebbly coarse sand. These coarser sediments were found to be located 3.5–4 km offshore Whangapoua beach to the west and southwest of Rakitu Island in 20–37 m water depth (Fig. 1), but may also occur elsewhere in the bay. These offshore gravels represent the most likely source for the Whangapoua gravel.

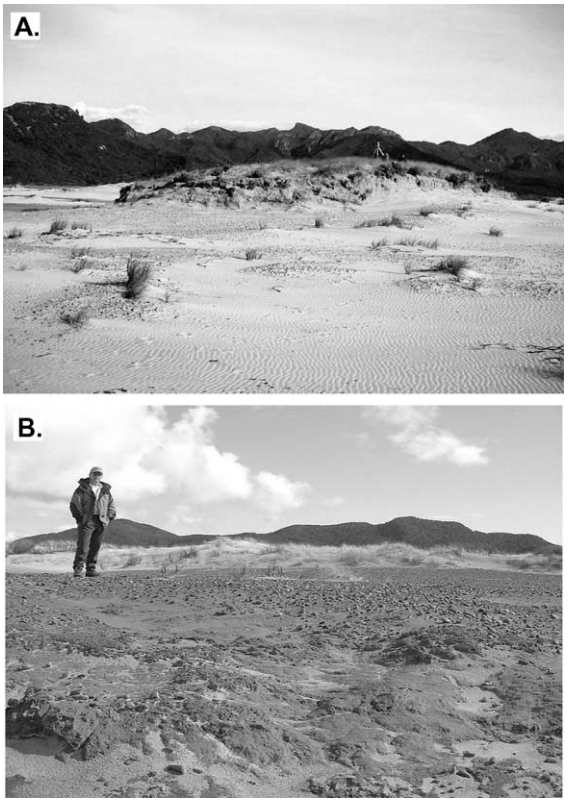

Fig. 5. (A) View of remnant of weathered Pleistocene dune sands that outcrop along the southern half of Whangapoua barrier. Midden B is located 5 m to the left (landward) of this Pleistocene outcrop. Note survey tripod for scale. (B) Whangapoua gravel mantling the surface of Pleistocene outcrop.

3. Methods

3.1. Mapping and analysis of Whangapoua dunes and gravel

The surface extent of the Whangapoua gravel outcrop was mapped using global positioning system (GPS) technology, with field data differentially corrected to reduce positional error to ±10 cm. The cross-shore profile of the beach and dunefield in the vicinity of the gravel sheet was surveyed using a "total station" instrument referenced to a local sea level datum determined from predicted high tide height and the actual position of high water on the day of survey. GPS and profile elevation data were combined to generate a three-dimensional surface representation of the central section of Whangapoua beach and dunes, with the Whangapoua gravel outcrop as an overlay.

The location of samples collected for grain size measurements are shown in Fig. 6. Analysis of sediment texture involved separate techniques for the sand and gravel fractions sampled from Whangapoua beach and dunes. First, grain size of beach and dune sands collected at 10 m intervals along nine cross-shore profiles spaced 30 m apart, plus that of the optical dating samples, was determined using a laser particle sizer (Galai™ CIS-100). This instrument employs the time-of-transition principle, whereby the larger the particle diameter the longer the time-of-transition across the laser beam path. For this analysis, approx-

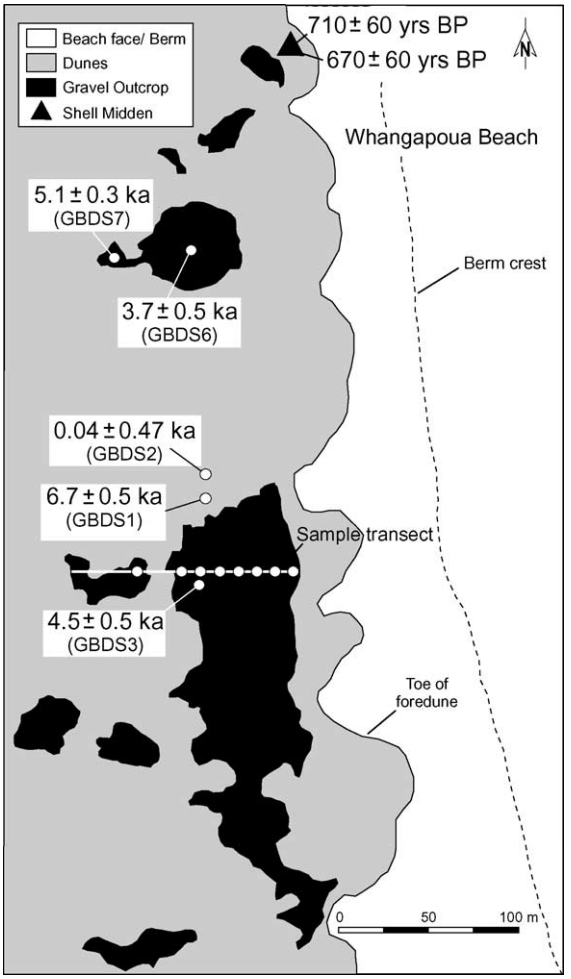

Fig. 6. Map showing locations and results of optical dating of dune sand and radiocarbon dating of midden shell, Whangapoua barrier. New Zealand Map Grid (Sheet S08 and T08) coordinates as follows: GBDS1 and GBDS2 60733N, 28510E; GBDS3 60709N, 28527E; GBDS6 60887N, 28512E; GBDS7 60868N, 28479E; Midden A 60994N, 28560E; Midden B 60072N, 28650E (not shown). The locations of samples collected for grain size analysis are also shown.

imately 1 g of sample was introduced to a solution of filtered water with GALAI data collection set to the 99% confidence level. Results reported here (Table 1) are for grain size expressed as percent of total particle volume. Second, eight bulk samples of Whangapoua gravel were collected at 10 m intervals along a representative cross-dune profile and measured for grain size by dry-sieving at half phi intervals from −1 to −5 phi. Grain size summary statistics were calculated using graphical methods (Folk, 1974). Third, the sizes of 140 pebble and cobble clasts were measured with sampling oriented along four representative cross-dune profiles divided into sampling stations positioned on the lower dune, mid-dune, dune crest and leeward dune face. Size data (long, intermediate, short axes) were used to calculate a sphericity index (Sneed and Folk, 1958) and to classify clast shape following the scheme of Zingg (1935).

3.2. Geochronology

Age limits on the time of deposition of the Whangapoua gravel come from optical dating (OSL) of associated dune sand and from radiocarbon dating of marine shells in midden deposits. The locations of the optical dating and radiocarbon samples are shown in Fig. 6.

Five samples of dune sand were collected for optical dating. Two samples were taken from a pit

Table 1
Summary grain size statistics for sand and gravel fraction of samples from Whangapoua beach and dunes, including samples used for optical dating

Size fraction	Sample position (m)	Mean (mm)	% Silt	Sorting (phi)
Sand	Berm	0.34	0.70	Moderate (0.93)
	10	0.17	1.67	Moderate (0.60)
	20	0.13	8.05	Moderate (0.63)
	30	0.18	1.57	Moderate (0.56)
	40	0.19	1.49	Moderate (0.59)
	50	0.19	1.71	Moderate (0.57)
	60	0.18	1.94	Moderate (0.54)
	70	0.17	1.37	Moderate (0.55)
	80	0.18	1.23	Moderate (0.51)
Gravel (granules and pebbles)	10	15.9	–	Very poor (2.10)
	20	13.2	–	Moderate (0.68)
	30	11.8	–	Very poor (3.20)
	40	12.4	–	Very poor (2.86)
	50	11.3	–	Very poor (3.35)
	60	17.1	–	Poor (1.88)
	70	13.9	–	Very poor (3.37)
	80	16.4	–	Poor (1.88)
Optical dating samples	GBDS1	0.32	0.64	Moderate (1.00)
	GBDS2	0.28	1.02	Moderate (1.00)
	GBDS3	0.23	1.12	Moderate (0.89)
	GBDS6	0.29	0.90	Moderate (0.98)
	GBDS7	0.26	0.84	Moderate (0.93)

Sample locations are shown on Fig. 8.

Table 2
Equivalent doses (D_{eq}), b values, dose rates, and apparent optical ages

Sample	D_{eq} (Gy)	b value (Gy μm^2)[a]	Depth (cm)[b]	D_T (Gy ka^{-1})[c]	Optical age (ka)[d]
GBDS1	6.74 ± 0.46	1.08 ± 0.07	20	1.10 ± 0.04	6.7 ± 0.5
GBDS2	0.044 ± 0.52	1.0 ± 0.1	–	1.00 ± 0.04	0.04 ± 0.47
GBDS3	5.63 ± 0.51	1.0 ± 0.1	55	1.25 ± 0.06	4.5 ± 0.5
GBDS6	4.55 ± 0.60	0.89 ± 0.06	38	1.23 ± 0.05	3.7 ± 0.5
GBDS7	6.23 ± 0.32	1.04 ± 0.04	47	1.23 ± 0.06	5.1 ± 0.3

[a] b value (α efficiency) as defined by Huntley et al. (1988); values for samples GBDS2 and GBDS3 are estimates.
[b] Depth below Whangapoua gravel layer. Sample GBDS2 was collected from a modern dune, 13 cm above the gravel.
[c] D_T: total dose rate (that due to cosmic rays plus that due to γ, β, and α radiation). For each sample, an estimate of 0.15 ± 0.02 Gy ka^{-1} was used for the cosmic-ray dose rate.
[d] Error terms are 1σ, and indicate analytical uncertainties, and uncertainty in burial depths, only.

excavation at the base of a 5-m-high dune that had developed over the Whangapoua gravel. These samples, GBDS1 and GBDS2, were collected 20 cm below and 13 cm above the gravel, respectively, with the intention of deriving an age bracket for the enclosed Whangapoua gravel. In addition, three samples were taken from shallow pits excavated into the older brown dune sand where it directly underlies the exposed gravel sheet. These included samples GBDS3, GBDS6 and GBDS7 taken 55, 38 and 47 cm below the Whangapoua gravel, respectively (Table 2). Field and laboratory procedures related to optical dating are detailed in Appendix A.

Radiocarbon dating of four specimens of articulated bivalve shells (*Paphies subtriangulatum*) collected from two Maori midden deposits on Whangapoua barrier (Table 3) was undertaken in order to establish an age estimate for Maori occupation, and to compare with optical ages on dune sands. Midden A is situated at the northern limit of exposed Whangapoua gravel and comprises a steep-sided dune that rises to about 6 m above surrounding dunes and is covered with shell (including articulated bivalves) to a thickness of approximately 50 cm (Fig. 4). A collection of hearth stones rest largely undisturbed on the crest of the midden. Midden B is located 400 m south of the main area of Whangapoua gravel deposits, on the lower elevation part of the dunefield. The midden is 5 m landward of an outcrop of Pleistocene sand that is mantled by granules, pebbles and cobbles. Four articulated shell samples (two from each midden) were submitted to the University of Waikato Radiocarbon Dating Laboratory for conventional assay. Radiocarbon ages reported here have been calibrated using CALIB version 4 (Stuiver et al., 1998a,b), based on the marine dataset, and incorporate a regional marine reservoir correction of −30 ± 15 years.

4. Results

4.1. Sediment texture

Beach and dune sediments at Whangapoua Bay comprise moderately sorted, fine to medium sand (mean diameter: 0.13–0.34 mm), with negligible difference between each depositional environment

Table 3
Radiocarbon ages of marine shells sampled from dune middens

Site	Material	Lab code	Conventional radiocarbon age (years BP)	Calibrated age range (AD)[a]
Midden A	Articulated marine shell *Paphies subtriangulatum*	Wk-6681	710 ± 60	1510–1640
Midden A	Articulated marine shell *Paphies subtriangulatum*	Wk-6682	670 ± 60	1530–1670
Midden B	Articulated marine shell *Paphies subtriangulatum*	Wk-8023	840 ± 70	1390–1535
Midden B	Articulated marine shell *Paphies subtriangulatum*	Wk-8026	720 ± 60	1500–1630

[a] Calibrated age calculated at 1σ level, using CALIB version 4.3 (Stuiver et al., 1998a,b), incorporating a marine reservoir correction of −30 ± 15 years.

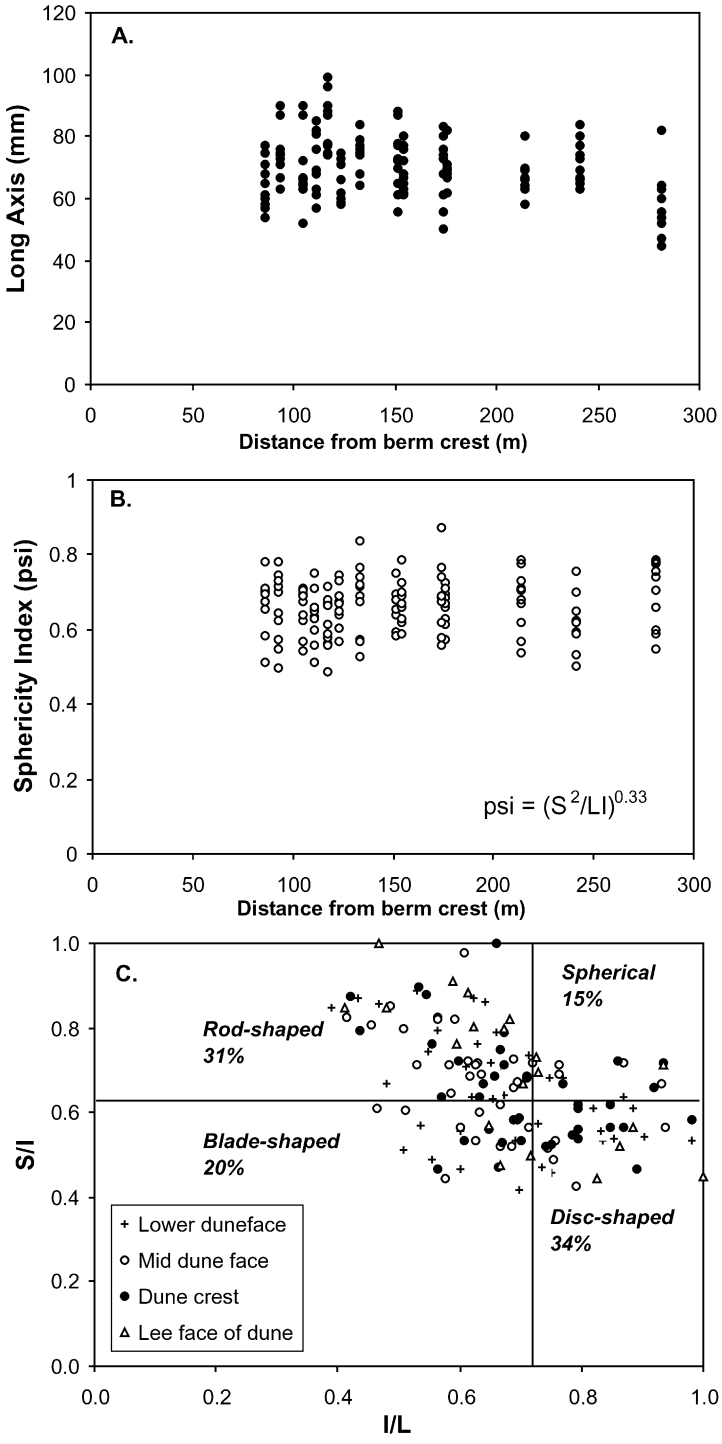

Fig. 7. Sediment texture data for the pebble to cobble fraction of the Whangapoua gravel, showing (A) clast size, (B) sphericity index, and (C) particle shape plots for 140 clasts sampled along four cross-shore profiles (shown in Fig. 3).

(Table 1). In addition, there is no discernible textural difference between the sands forming active dunes and the older brown dune sand found directly beneath the gravel. All optical dating samples are classified as moderately sorted, fine to medium sand (mean diameter: 0.23–0.32 mm).

The Whangapoua gravel consists of clasts that range in size from coarse granules to cobbles. Mean grain size of the granule and pebble fraction ranges from 11.3 to 17.1 mm diameter, and all samples are poorly to very poorly sorted, with no discernible cross-dune trends in particle size (Table 1). Similarly, within the cobble fraction there is no obvious landward-fining trend, with long-axis length ranging from 45 to 100 mm (Fig. 7A), although there is a slight concentration of pebbles with long axes less than 60 mm long on the lee face of the foredune. Sphericity index values for the pebble and cobble fraction range from 0.49 to 0.87 (mean: 0.66 ± 0.07) (Fig. 7B), and the great majority of clasts are sub-rounded to rounded (Fig. 2D). Particle shape data disclose a slight bias toward disc-shaped (34%) and rod-shaped (31%) clasts over blade-shaped (20%) and spherical (15%) forms, but on the basis of these criteria there is no spatial organisation of particles across the dune face (Fig. 7C).

A striking characteristic of many of the greywacke clasts is a distinct weathering varnish on the exposed surface that is not evident on the underside (Fig. 8), indicating prolonged subaerial exposure (hence no dune burial) and minimal reworking of these particular clasts. Directly beneath larger clasts, we also noted a millimetre-thick bed of heavy mineral sands that in turn rest unconformably upon brown dune sands, indicating hydraulic sorting and scour of dune sands in association with gravel deposition. In summary, the Whangapoua gravel is a very poorly sorted scatter of very coarse clasts that appear to have remained largely undisturbed since deposition and are in erosional contact with underlying dunes.

The lithologic composition of the Whangapoua gravel is dominated by greywacke (>80%) and thin-

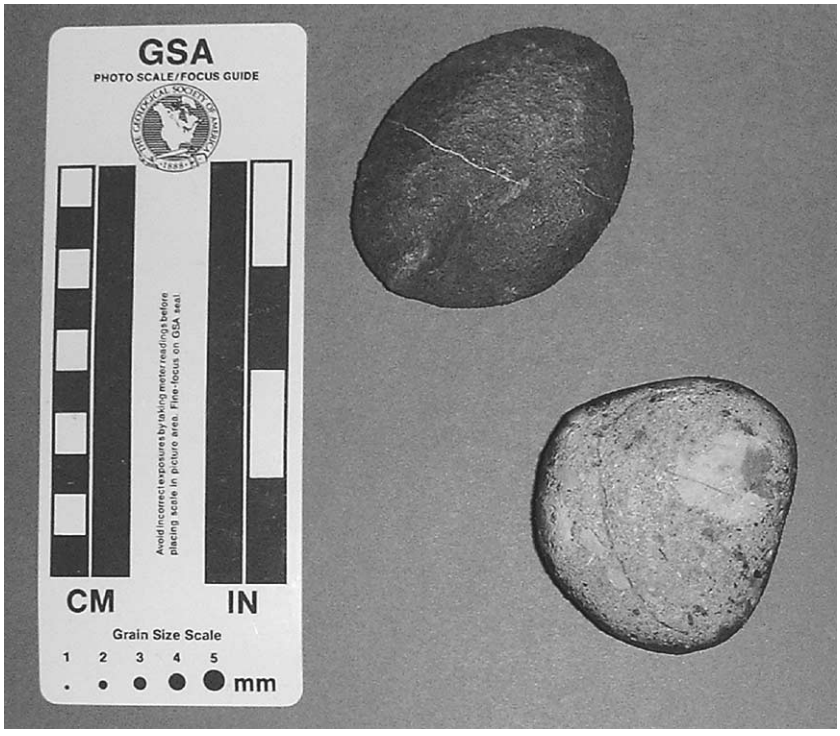

Fig. 8. Photograph of two greywacke pebbles showing weathered varnish surface of the exposed surface (upper clast) and the non-weathered underside (lower clast).

bedded argillite, with minor amounts (5–10%) of rhyolite, andesitic breccia, tuff and agglomerate. These rock types are all found in the hinterland to Whangapoua Harbour and outcrop on the headlands at each end of the bay. However, because the Whangapoua dunes are not in direct connection with hillslopes or streams, the only probable gravel source is the nearshore to inner shelf of Whangapoua bay. Pumice clasts (pebble to cobble size) also form part of the gravel sheet and are presumably sea-rafted. These include material that is consistent in appearance with Loisels Pumice (light to dark brown-grey and flow banded; Wellman, 1962) and other rare clasts (light brown-grey and non-banded) that have similar mineralogy (hypersthene dominated ferromagnesium; P. Shane, personal communication) to Taupo Tephra (1.85 ka BP; Froggatt and Lowe, 1990). The Loisels-style pumice is more prevalent than the Taupo(?) pumice and is concentrated toward the toe (lower 3–5 m) of the gravel sheet. Loisels Pumice has previously been reported from the east coast of Great Barrier Island (Pullar et al., 1977; McFadgen, 1985) and has an age range of ca. 1.5–0.6 ka BP, based on radiocarbon dating from several North Island sites (Shane et al., 1998).

4.2. Optical ages of Whangapoua dune sands

Optical ages for the dune sand below the Whangapoua gravel range from 6.7 ± 0.5 ka (GBDS1) to 3.7 ± 0.5 ka (GBDS6), and are detailed in Table 2 (Fig. 6). Although the calculated optical ages for this unit are statistically consistent, any difference probably reflects different burial times of sands as a result of local aeolian reworking (i.e., cut and fill) prior to being covered by Whangapoua gravel. The optical age for the sample collected from the base of a $\sim$ 5-m-high dune (sample GBDS2), 13 cm above Whangapoua gravel, yielded an age of 0.04 ± 0.47 ka.

The optical ages therefore indicate that Whangapoua gravel was deposited sometime between 4.7 ka and the present, if the analytical uncertainty associated with the optical age of sample GBDS6 (the youngest age) is considered at $+2\sigma$.

It should be noted that anomalous fading was not corrected for in our samples. The reason for this is that the intensity of the luminescence emitted from our samples was too low to produce useable fading rates. Therefore, despite our 38-day delay between laboratory irradiation and the final measurements (Fig. A1), it is likely that our calculated ages are too young. However, based on previous studies of North Island samples (e.g., Lian and Shane, 2000) it is expected that the true ages lie within the age range defined by our analytical uncertainties.

4.3. Radiocarbon ages of middens

Four radiocarbon age estimates on samples of articulated marine shells from two middens yield calibrated ranges which all overlap at 1σ, collectively spanning the years 1390–1670 AD (Table 3). These shells formed part of Maori midden deposits on the Whangapoua dunes, and their ages can only be used to indicate the time of human activity at that particular midden. Indeed, the history of Maori occupation at Whangapoua may pre-date the oldest radiocarbon age reported here. Of greater relevance, however, is the fact that cobble-sized hearth stones are scattered throughout the Whangapoua gravel, and midden shells are dispersed landward from primary middens. This reworking suggests that these materials were incorporated into the transport load when the gravel was deposited onto the dunes. If we accept this proposition, then the event that deposited the Whangapoua gravel occurred during, or after, the period 1390–1670 AD.

5. Discussion

We recognise three possible natural mechanisms for the transport and deposition of the Whangapoua gravel; (i) incident wave run-up associated with storm surge, (ii) concentration by aeolian winnowing, and (iii) tsunami run-up. Of these, storm surge and wind winnowing are considered the least likely mechanisms, as explained below.

The Whangapoua gravel is deposited to an elevation (14.3 m) that is well above the maximum recorded storm surge height for the northeast coast of North Island; reported as 0.8 m above mean high water springs (plus 2–4 m breaking wave height) at Bream Bay in July 1978 (Hume, 1979). Not only is the Whangapoua gravel beyond storm limits, it is an improbable record of storm surge because such events

are more erosional in their geomorphic impact than depositional. While storm erosion may leave a lag of coarse-grained sediment, observation of the post-storm beach at Whangapoua indicates that this lag takes the form of a layer of heavy mineral sand deposited on a flatter beachface. Storm waves are certainly not capable of transporting pebble to cobble-sized sediment to the crest of ~ 15-m high dunes.

Aeolian sorting processes commonly produce concentrations of the coarse-grained fraction of dune deposits, notably on the surface of deflation basins and dune slacks (or swales) (Hesp and Thom, 1990). However, the initial placement of the coarse-grained fraction in dunes is typically via a non-aeolian mechanism (i.e., storm surge, spring tide swash) and moreover, is restricted to lower dune surfaces. At Whangapoua Bay, the lower elevation deflation surfaces along the southern half of the barrier are indeed mantled by localised gravel concentrations of granule to pebble size, mixed with shell. The transport mechanism in these areas is undoubtedly wave run-up during storm surge, because these surfaces are within the range of known storm surge heights for this coast. The presence of flotsam (e.g., bottles, rope) mixed with these deposits also indicates frequent inundation. However, as already argued the higher elevation gravel deposit on Whangapoua dunefield is beyond the reach of storm surge. The majority of clasts (pebble-cobble sized) are simply too large for aeolian transport in this environment.

Tsunami run-up remains the only plausible mechanism that can account for the position and character of the Whangapoua gravel sheet. The absence of cross-shore trends in clast texture is consistent with rapid deposition by water flowing as a turbulent flow that surged across the beach and dunes. Presumably, sand was incorporated in the tsunami transport load but the only evidence for this is the thin bed of heavy mineral sand that lies directly below the gravel and above the older weathered dune sands. The range of optical ages on these dune sands (6.7 ± 0.5 to 3.7 ± 0.5 ka) support the interpretation that the gravel is in erosional contact with the dunes. Because the Whangapoua gravel is only one-grain thick it is not possible to distinguish between tsunami run-up and backwash, so we assume that the erosional surface across the dunes and the gravel deposit are the integrated product of both mechanisms. The uniform textural character of the gravel sheet and absence of runnels in the dunes suggest, however, that backwash was minimal and that the dunefield was probably overwashed by tsunami run-up.

An important feature of the interpreted tsunami run-up deposit at Whangapoua Bay is the spatial variability in the distribution of deposits, which provides a useful record of the complexity of tsunami behaviour on coasts. Any interpretation of patterns in tsunami inundation that is based on depositional evidence must assume negligible reworking of primary deposits. In the Whangapoua case, preservation of the original form of tsunami deposits is considered highly likely given the coarse-grained texture and position beyond the limit of storm wave run-up. Reworking associated with dune lowering via aeolian processes is possible but unlikely given the absence of blowouts in the vicinity of the gravel sheet. Burial is also possible but this would simply serve to enhance the preservation potential of the gravel. Therefore, the present distribution of the gravel provides a good indication of the spatial complexity of tsunami run-up. The position and elevation of the primary gravel deposit suggests maximum run-up occurred toward the central section of Whangapoua beach. We suggest this is a product of wave diffraction and/or refraction around Rakitu Island, leading to wave focusing in the centre of Whangapoua Bay (constructive interference with ocean swell may also have increased wave amplitude locally). The absence of gravel deposits along the northern half of the Whangapoua dunefield supports this proposition. Along the southern half of Whangapoua dunes, the gravel is localised in dune slacks and perched on eroded bench remnants of Pleistocene dunes. The lower elevation of this part of the dunefield would have allowed greater inland incursion of the tsunami, possibly resulting in landward redistribution of dune sands. This destructive form of tsunami impact on coastal barriers has been documented elsewhere for historical tsunami events on the coasts of Portugal and Japan (Dawson, 1994, 1996). Recovery of core samples from the subtidal deposits in Whangapoua Harbour to test for tsunami evidence further landward is planned for the next phase of our research.

Identifying a specific generating mechanism for the tsunami is difficult, with both local and far-field (trans-Pacific) generation possible. We focus here on

local events that may have generated a tsunami and note that there are several possibilities in the time frame established by our dating program. The logical option is submarine volcanism and/or associated earthquake activity in the vicinity of the Hikurangi trough, located 360 km to the east–southeast of Great Barrier Island (Fig. 1). This is a seismically active area associated with the subduction zone between the Australian and Pacific plates for which Berryman et al. (1989) document a minimum of 21 paleoseismic events during the past 2.5 ka that affected eastern coasts of North Island. The moment magnitude of these events are estimated to have ranged from 7.3 to 8.0, based on the dimensions of coastal uplift along the east coast and modelling of the 1931 Napier earthquake (Berryman et al., 1989). It is reasonable, therefore, to infer that the tsunami that deposited the Whangapoua gravel may have been generated by one of these paleoseismic events in the Hikurangi trough.

An equally credible source area is the southern Kermadec arc which comprises 13 modern submarine volcanoes between 34°50′ S and 36°50′ S (Fig. 1) (Wright and Gamble, 1999). Of these volcanoes, the Healy caldera is a strong candidate for tsunami generation. On the basis of detailed analysis of pumice geochemistry and vesicularity, Wright et al. (in press) provide compelling evidence that the eruption of Healy was pyroclastic (rather than effusive) and suggest that the associated caldera collapse in 550–1000 m water-depth was catastrophic and possibly tsunamigenic. Further, the pumice produced by the Healy eruption has a similar geochemistry and flow structure to Loisels Pumice (Shane et al., 1998; Wright et al., in press), a widely distributed sea-rafted pumice found along the northeast coast of New Zealand, including Great Barrier Island (Pullar et al., 1977; McFadgen, 1985). Recognising that sea-rafted pumice would take weeks to months to be transported the ~370 km from Healy caldera to Great Barrier Island and therefore arrive well after a tsunami, it is possible that the pumice found within the Whangapoua gravel was derived from the Healy eruption. The age of Loisels Pumice has been debated in the literature, with the ca. 1500–600 years BP range now recognised to be a function of some ^{14}C age estimates being associated with reworked deposits (Shane et al., 1998). Taking this into account, McFadgen (1994) reviewed the published ages for Loisels Pumice and argues for a calibrated age range of 660–510 years BP (1290–1440 AD). If our interpretation that middens at Whangapoua have been disturbed by tsunami run-up is correct, then the age of these middens (1390–1670 AD) coincides with this revised age for Loisels Pumice (McFadgen, 1994), and by inference the Healy eruption. At the very least, the age range for all these events lies within the 3.7 ± 0.5 to 0.04 ± 0.47 ka optical age bracket we have established for the Whangapoua gravel.

6. Conclusion

The Whangapoua gravel presents strong evidence for an interpretation of tsunami inundation over coastal dunes to elevations well above maximum-recorded storm surge height for the northeast coast of North Island, New Zealand. The effects of tsunami run-up and backwash are integrated as a record of erosion of mid-Holocene dunes and deposition of a poorly sorted granule to cobble lag that has subsequently armoured the bed, largely preserving the erosional morphology. Local bathymetry and topography appear to have favoured focusing of tsunami energy and availability of an offshore supply of coarse-grained sediment has allowed preservation of a distinct sedimentological signature. This combination of local factors may explain why other similar examples of tsunami run-up have not been reported for the northeast coast of North Island, as we would expect this event to have impacted other coastal areas in the region. As this is the first documented case of tsunami impact on subaerial coastal environments for the coast of New Zealand, it may be the case that other analogous tsunami deposits await to be recognised.

Acknowledgements

This work was funded in part by grants from the National Geographic Society (Research and Exploration Committee, Grant No. 6075-97) and Auckland University Research Committee. We thank John Ogden (University of Auckland) for first suggesting we examine the Whangapoua gravel deposit. Ningsheng Wang and Ed Butler (Victoria University of Wellington) assisted with sample preparation for

optical dating measurements, Phil Shane (University of Auckland) provided pumice analysis, and Catherine Chagué-Goff (National Institute of Water and Atmospheric Research), James Goff (GeoEnvironmental Consultants) and Martin Scott (University of Auckland) gave valuable field assistance. Curt Peterson, Edward Bryant and Keith Crook are thanked for their comments on the original manuscript.

Appendix A. Optical Dating Procedures

Optical dating is a method by which the time elapsed since quartz or feldspar grains were last exposed to light can be determined. The details of the method can be found in, for example, Aitken (1998), Lian and Huntley (2001), and the papers published in *Radiation Measurements* (Vol. 27 5/6, 1997).

Sampling of the modern dune sand, and the older brown dune sand, was from freshly excavated pits using 30-cm long aluminium tubes which were inserted into the pit walls. The sample tubes were carved out from the pit walls and immediately sealed to retain moisture.

Sample tubes were opened in the laboratory under subdued orange light, and about 500 g (moist mass) of material was extracted from near the centre of each tube. From this, approximately 30 g was removed, dried, and milled to a fine powder to be used later for dosimetry. The remaining sample was treated using standard methods (e.g., Wintle, 1997; Lian and Huntley, 1999), and the 4–11 μm diameter (fine silt) polymineral fraction was separated and deposited onto 1-cm diameter aluminium discs; for each sample about 50 such aliquots were made. The fine silt fraction was chosen because our laboratory β source was more accurately calibrated to this size fraction.

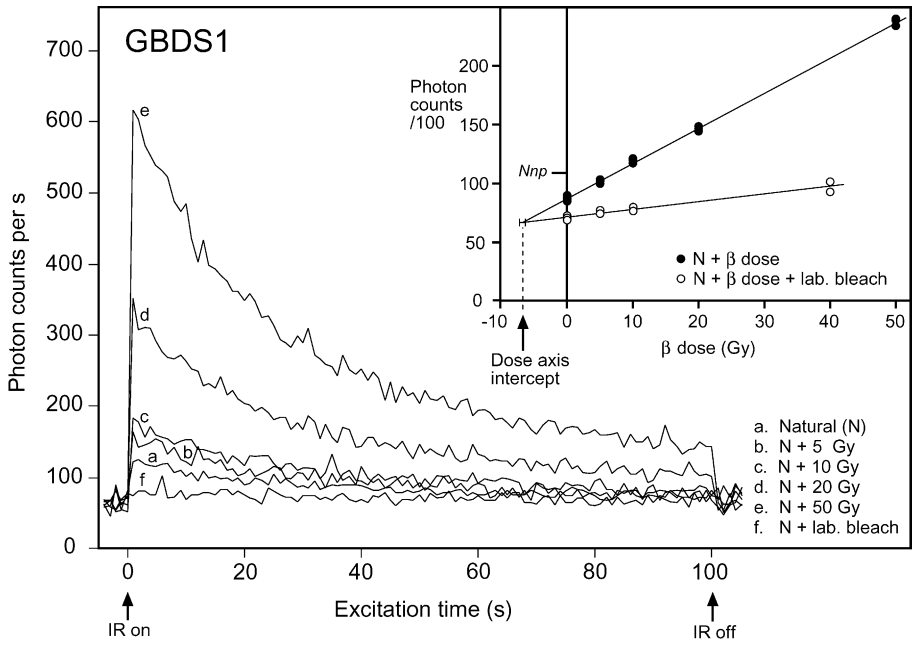

Fig. A1. Luminescence decay (main figure) and dose response data (inset) for sample GBDS1. After laboratory irradiation, the sample aliquots were stored for 24 h, then preheated at 140 °C for 7 days, stored for a further 30 days, and then measured at room temperature under infrared (IR) excitation (~ 20 mW cm^{-2} of 1.4 eV, 800–960 nm, photons at the sample) for 100 s. The measured luminescence was of energy ~ 3.1 eV (400 nm, violet) from the excitation of K-feldspar. Luminescence was detected using a EMI 9235QA photomultiplier tube mounted behind a Schott BG-39 (IR absorbing) and a Kopp 5–58 (blue-pass) optical filter. The inset shows the β response using the luminescence integrated over the entire excitation period; each data point is the average of several determinations. The data were normalized using the equal predose method (Aitken, 1998, p. 96). The additive dose data (solid circles) and the thermal-transfer correction data (open circles) were fitted with straight lines using maximum likelihood. The equivalent dose is obtained from the intercept (dose axis intercept) of the two fitted curves.

Table A1
K, U, and Th concentrations determined from laboratory analyses and water contents

Sample	K (%)[a]	Th (μg g^{-1})[b]	U (μg g^{-1})[c]	Water contents[d]		
				Δ^{w}_{ac}	Δ^{w}_{sat}	Δ^{w}
GBDS1	0.49 ± 0.02	2.2 ± 0.2	0.55 ± 0.06	0.074	0.196	0.074 ± 0.010
GBDS2	0.41 ± 0.02	2.0 ± 0.2	0.53 ± 0.06	0.052	0.202	0.052 ± 0.010
GBDS3	0.47 ± 0.02	3.2 ± 0.3	0.64 ± 0.06	0.043	0.199	0.043 ± 0.010
GBDS6	0.52 ± 0.03	3.0 ± 0.3	0.58 ± 0.06	0.039	0.212	0.039 ± 0.010
GBDS7	0.44 ± 0.02	2.6 ± 0.3	0.73 ± 0.06	0.021	0.177	0.021 ± 0.005

[a] From inductively coupled-plasma atomic emission spectrometry.
[b] From delayed neutron counting.
[c] From neutron activation analysis.
[d] Δ^{w}_{ac} and Δ^{w}_{sat}, are the as collected and saturated water contents, respectively; Δ^{w} is the water content used for the dose rate calculation. Water content=(mass water)/(mass dry minerals).

Silt content (measured by volume) in each sample is listed in Table 1.

Equivalent doses were determined using the additive-dose method, with thermal transfer correction (Huntley and Lian, 1999; Lian and Huntley, 1999); an example is shown in Fig. A1. The laboratory apparatus used for all the measurements was the same as that used by Lian and Shane (2000).

For each sample, the environmental dose rate due to α, β and γ radiation was calculated from the concentrations of U, Th, and K using standard formulae (e.g., Aitken, 1985), but with the updated dose-rate conversion factors of Adamiec and Aitken (1998) (Table A1). For samples near the surface, a significant part of the environmental dose rate comes from cosmic rays, but this contribution decreases rapidly with burial depth. Although the cosmic-ray dose rate can be calculated in detail (see Prescott and Hutton, 1994), knowledge of periods of erosion and deposition at our sample sites is lacking. Indeed, the surface on which the Whangapoua gravel was deposited is hummocky, and partially occupied by transient dunes, some several metres high. While at the surface, the samples would have received a dose of about 0.3 Gy ka^{-1} from cosmic rays (about 25% of the total dose rate), but at their present burial depths cosmic rays would have contributed only 10–15% of the total dose rate, depending on whether a sample site was covered by a transient dune, or not. Furthermore it is not known how much material was eroded at each sample site during the event that deposited the gravel. The cosmic ray dose rate was therefore estimated using a burial depth of 2 m, with an uncertainty that is expected to account for any reasonable change at 2σ (Table A1).

The presence of water in the sediment matrix reduces the radiation dose to the minerals, and this has to be accounted for when calculating the environmental dose rate. Since all of our samples were collected from well-drained sands, we used the "as-collected" water content in the calculations with an uncertainty that is expected to account for wet and dry periods at 2σ (Table A1).

Optical ages were calculated by dividing the equivalent dose by the environmental dose rate and are shown in Table 2.

References

Adamiec, G., Aitken, M.J., 1998. Dose-rate conversion factors: update. Ancient TL 16, 37–50.

Aitken, M.J., 1985. Thermoluminescence Dating. Academic Press, London.

Aitken, M.J., 1998. An Introduction to Optical Dating. Oxford Univ. Press, Oxford.

Atwater, B.F., 1987. Evidence for Holocene earthquakes along the outer coast of Washington state. Science 236, 942–944.

Atwater, B.F., Nelson, A.R., Clague, J.J., Carver, G.A., Yamaguchi, D.K., Bobrowsky, P.T., Bourgeois, J., Darienzo, M.E., Grant, W.C., Hemphill-Haley, E., Kelsey, H.M., Jacoby, G.C., Nishenko, S.P., Palmer, S.P., Peterson, C.D., Reinhart, M.A., 1995. Summary of coastal geologic evidence for past great earthquakes at the Cascadia subduction zone. Earthquake Spectra 11, 1–18.

Berryman, K.R., Ota, Y., Hull, A.G., 1989. Holocene paleoseismicity in the fold and thrust belt of the Hikurangi subduction zone, eastern North Island, New Zealand. Tectonophysics 163, 185–195.

Bryant, E., Young, R.W., Price, D.M., 1992. Evidence of tsunami

sedimentation on the southeastern coast of Australia. Journal of Geology 100, 753–765.
Bryant, E., Young, R.W., Price, D.M., 1996. Tsunami as a major control on coastal evolution, southeastern Australia. Journal of Coastal Research 12, 831–840.
Cita, M.B., Camerlenghi, A., Kastens, K.A., McCoy, F.W., 1984. New findings of Bronze Age homogenites in the Ionian Sea: geodynamic implications for the Mediterranean. Marine Geology 55, 47–62.
Clague, J.J., 1997. Evidence for large earthquakes at the Cascadia subduction zone. Reviews of Geophysics 35, 439–460.
Clague, J.J., Bobrowsky, P.T., Hutchinson, I., 2000. A review of geological records of large tsunamis at Vancouver Island British Columbia, and implication for hazard. Quaternary Science Reviews 19, 849–863.
Dawson, A.G., 1994. Geomorphological effects of tsunami run-up and backwash. Geomorphology 10, 83–94.
Dawson, A.G., 1996. The geological significance of tsunamis. Zeitschrift für Geomorphologie Supplementband 102, 199–210.
Dawson, A.G., Hindson, R., Andrade, C., Freitas, C., Parish, R., Bateman, M., 1995. Tsunami sedimentation associated with the Lisbon earthquake of 1 November AD 1755: Boca do Rio, Algarve, Portugal. The Holocene 5, 209–215.
Folk, R.L., 1974. Petrology of Sedimentary Rocks, 3rd edn. Hemphills, Austin, TX.
Froggatt, P.C., Lowe, D.J., 1990. A review of late Quaternary silicic and some other tephra formations from New Zealand: their stratigraphy, nomenclature, distribution, volume and age. New Zealand Journal of Geology and Geophysics 33, 89–109.
Gibb, J.G., 1986. A New Zealand regional Holocene eustatic sea-level curve and its application to determination of vertical tectonic movements. Royal Society of New Zealand, Bulletin 24, 377–395.
Goff, J.R., Chagué-Goff, C., 1999. A late Holocene record of environmental changes from coastal wetlands: Abel Tasman National Park, New Zealand. Quaternary International 56 (1), 39–51.
Goff, J.R., Rouse, H.L., Jones, S.L., Hayward, B.W., Cochran, U., McLea, W., Dickinson, W.W., Morley, M.S., 2000. Evidence for an earthquake and tsunami about 3100–3400 yr ago, and other catastrophic saltwater inundations recorded in a coastal lagoon, New Zealand. Marine Geology 170 (1–2), 231–249.
Hayward, B.W., Brook, F.J., Grace, R.V., Bull, V.H., 1982. Soft bottom macrofauna and sediments off Rakitu Island, north–east New Zealand. Tane 28, 149–162.
Hayward, B.W., Grace, R.V., Francis, M.P., 1986. Sediments and benthos of northeastern Great Barrier Island, New Zealand. Journal of the Royal Society of New Zealand 16, 347–355.
Hesp, P.A., Thom, B.G., 1990. Geomorphology and evolution of active transgressive dunefields. In: Nordstrom, K.F., Psuty, N.P., Carter, R.W.G. (Eds.), Coastal Dunes: Form and Process. Wiley, New York, pp. 253–288.
Hume, T.M., 1979. Factors contributing to coastal erosion on the east coast of Northland during July 1978. Internal Report, Water and Soil Section, New Zealand Ministry of Works and Development, 25 pp.
Huntley, D.J., Lian, O.B., 1999. Using optical dating to determine when a sediment was last exposed to sunlight. In: Lemmen, D.S., Vance, R.E. (Eds.), Holocene Climate and Environmental Change in the Palliser Triangle: A Geoscientific Context for Evaluating the Impacts of Climate Change on the Southern Canadian Prairies. Geological Survey of Canada Bulletin, vol. 534, pp. 211–222.
Huntley, D.J., Berger, G.W., Bowman, S.G.E., 1988. Thermoluminescence responses to alpha and beta irradiations, and age determination when the high dose response is nonlinear. Radiation Effects 105, 279–284.
Lian, O.B., Huntley, D.J., 1999. Optical dating studies of post-glacial aeolian deposits from the south-central interior of British Columbia, Canada. Quaternary Science Reviews 18, 1453–1466.
Lian, O.B., Huntley, D.J., 2001. Luminescence dating. In: Last, W.M., Smol, J.P. (Eds.), Tracking Environmental Change Using Lake Sediments. Basin Analysis, Coring, and Chronological Techniques, vol. 1. Kluwer Academic Publishing, Dordrecht, The Netherlands, pp. 261–282.
Lian, O.B., Shane, P.A., 2000. Optical dating of palaeosols bracketing the widespread Rotoehu tephra, North Island, New Zealand. Quaternary Science Reviews 19, 1649–1662.
Lowe, D.J., de Lange, W.P., 2000. Volcano-meteorological tsunamis, the c. AD 200 Taupo eruption (New Zealand) and the possibility of a global tsunami. The Holocene 10 (3), 401–407.
McFadgen, B.G., 1985. Late Holocene stratigraphy of coastal deposits between Auckland and Dunedin, New Zealand. Journal of the Royal Society of New Zealand 15, 27–65.
McFadgen, B.G., 1994. Archaeology and Holocene sand dune stratigraphy on Chatham Island. Journal of the Royal Society of New Zealand 24, 17–44.
McSaveney, M.J., Goff, J.R., Darby, D.J., Goldsmith, P., Barnett, A., Elliot, S., Nongkas, M., 2000. The 17 July 1998 tsunami, Papua New Guinea: evidence and initial interpretation. Marine Geology 170, 81–92.
Minoura, K., Nakaya, S., 1991. Traces of tsunami preserved in inter-tidal lacustrine and marsh deposits: some examples from northeast Japan. Journal of Geology 99, 265–287.
Minoura, K., Nakaya, S., Uchida, M., 1994. Tsunami deposits in a lacustrine sequence of the Sanriku coast, northern Japan. Sedimentary Geology 89, 25–31.
Prescott, J.R., Hutton, J.T., 1994. Cosmic ray contributions to dose rates for luminescence and ESR dating: large depths and long-term time variations. Radiation Measurements 23, 497–500.
Pullar, W.A., Kohn, B.P., Cox, J.E., 1977. Air-fall Kaharoa Ash and Taupo Pumice, and sea-rafted Loisels Pumice, Taupo Pumice, and Leigh Pumice in northern and eastern parts of the North Island, New Zealand. New Zealand Journal of Geology and Geophysics 20, 697–717.
Shane, P.A., Frogatt, P.C., Smith, I.E., Gregory, M., 1998. Multiple sources for sea-rafted Loisels pumice, New Zealand. Quaternary Research 49, 271–279.
Sneed, E.D., Folk, R.L., 1958. Pebbles in the lower Colorado River, TX: a study in particle morphogenesis. Journal of Geology 66, 114–150.
Stuiver, M., Reimer, P.J., Bard, E., Beck, J.W., Burr, G.S., Hughen, K.A., Kromer, B., McCormac, F.G., Van de Plicht, J., Spurk, M., 1998a. INTCAL98 Radiocarbon age calibration 24,000–0 cal BP. Radiocarbon 40, 1041–1083.

Stuiver, M., Reimer, P.J., Braziunas, T.F., 1998b. High-precision radiocarbon age calibration for terrestrial and marine samples. Radiocarbon 40, 1127–1151.

Takashimizu, Y., Masuda, F., 2000. Depositional facies and sedimentary successions of earthquake-induced tsunami deposits in Upper Pleistocene incised valley fills, central Japan. Sedimentary Geology 135, 231–239.

Thompson, B.N., 1960. Sheet 2B Barrier (1st Edition). Geological Map of New Zealand 1:250,000 scale. Department of Scientific and Industrial Research, Wellington, New Zealand.

Wellman, H.W., 1962. Holocene of the North Island of New Zealand: a coastal reconnaissance. Transactions of the Royal Society of New Zealand 1, 29–99.

Wintle, A.G., 1997. Luminescence dating: laboratory procedures and protocols. Radiation Measurements 27, 769–817.

Wright, I.C., Gamble, J.A., 1999. Southern Kermadec submarine caldera arc volcanoes (SW Pacific): caldera formation by effusive and pyroclastic eruption. Marine Geology 161, 207–227.

Wright, I.C., Gamble, J.A., Shane, P.A., in press. Submarine silicic volcanism of the Healy caldera, southern Kermadec arc (SW Pacific): I-volcanology and eruption mechanisms. Bulletin of Volcanology.

Yeh, H., Imamura, F., Synolakis, C., Tsuji, Y., Liu, P., Shi, S., 1993. The Flores Island tsunamis. Eos Transactions, American Geophysical Union 74 (33), 369–373.

Young, R., Bryant, E., Price, D.M., 1996. Catastrophic wave (tsunami?) transport of boulders in southern New South Wales, Australia. Zeitschrift fur Geomorphologie 40, 191–207.

Zingg, T., 1935. Beitrag zur Schotteranalyse. Schweizerische Mineralogische und Petrographische Mitteilungen 15, 39–140.